Original Research

neural press

Reduced modeling of pacemaker spiking in dorsal raphe nucleus and locus coeruleus neurons

Ying Zhou[1], Henry C. Tuckwell[2,*] and Nicholas J. Penington[3, 4]

[1]Department of Mathematics, Lafayette College, 1 Pardee Drive, Easton, PA 18042, USA
[2]School of Electrical and Electronic Engineering, University of Adelaide, Adelaide, South Australia 5005, Australia
[3]Department of Physiology and Pharmacology
[4]Program in Neural and Behavioral Science and Robert F. Furchgott Center for Neural and Behavioral Science, State University of New York, Downstate Medical Center, Box 29, 450 Clarkson Avenue, Brooklyn, NY 11203-2098, USA

***Corresponding author:** henrytuckwell@hotamil.com

https://doi.org/10.56280/1532965848

Submitted: 15 March 2022, Accepted: 15 June 2022, Published: 2 October 2022

Abstract

Many central neurons, particularly certain brainstem aminergic neurons, exhibit spontaneous and fairly regular spiking with frequencies of order a few Hz. Many ion channel types contribute to such spiking, so accurate modeling of spike generation requires solving very large systems of differential equations, ordinary in the first instance. Since the analysis of spiking behavior when many synaptic inputs are active adds further to the number of components, it is useful to have simplified mathematical models of spiking in such neurons so that, for example, inputs and output spike features trains can be incorporated, including stochastic effects. In this article, we consider a simple two-component model whose solutions can mimic features of spiking in serotonergic neurons of the dorsal raphe nucleus and noradrenergic neurons of the locus coeruleus. The model is of the Fitzhugh-Nagumo type, and solutions are computed with two representative sets of parameters. Frequency versus input currents reveals Hodgkin type 2 behavior, which is supported by bifurcation and phase plane analysis. The article concludes with a brief review of the previous modeling of these types of neurons and their relevance to serotonergic and noradrenergic involvement studies in certain cognitive processes and pathologies.

Keywords: Dorsal raphe nucleus, serotonergic neurons, locus coeruleus, noradrenergic neurons, computational model, pacemaker

1. Introduction

Neurons that exhibit (approximately) periodic spiking in the presumed absence of synaptic input are called autonomous pacemakers and include neurons found in the subthalamic nucleus, nucleus basalis, globus pallidus, raphe nuclei, cerebellum, locus coeruleus, ventral tegmental area, and substantia nigra [1].

To function as pacemakers, some cells may require small amounts of depolarizing inputs, natural or laboratory. Thus, for example, Pan et al. [2] found that all 42 rat LC neurons fired spontaneously. In contrast, Williams et al. [3] and Ishimatsu et al. [4] reported that most cells did not require excitatory input to fire regularly. These latter three sets of results were obtained in vitro. Sanchez-Padilla et al. [5] reported that spike rate in mouse LC neurons was not affected by blockers of glutamatergic or GABAergic synaptic input, supporting the idea that these cells were autonomous pacemakers.

The neurons with which we are mainly concerned are serotonergic neurons of the dorsal raphe nucleus and noradrenergic neurons of the locus coeruleus. The electrophysiological properties of these cells have been much investigated over the last several; decades [6,7,8,9]. Their roles in stress-related disorders such as MDD and PTSD by means of reciprocal interactions with, inter alia, the HPA axis (especially through the PVN), hippocampus and prefrontal cortex are well documented [10,11,12,13]. For example, CRH neurons of the PVN project directly to SE neurons of the DRN [14] and NA neurons of the LC [15]. Stress, via upregulation of the cAMP pathway, increases the excitability of LC neurons [16]. In addition, these brainstem neurons are endowed with glucocorticoid receptors activated by high levels of corticosterone (cortisol) [17].

Journal of Multiscale Neuroscience

In most common experimentally employed animals except the cat, the locus coeruleus is almost completely homogeneous, consisting of noradrenergic neurons, which in rats number about 1500 [18,19]. The number of neurons in the rat DRN is between 12000 and 15000 [20, 21], of which up to 50% are principal serotonergic cells [22]. There are about 1000 dopaminergic cells [23] and GABAergic cells, whose density varies throughout the divisions of the nucleus, as well as several other types of neurons.

The SE neurons of the DRN and the NA neurons of the LC often exhibit a slow regular firing pattern with frequencies of order 0.5 to 2 Hz in slice and sometimes higher in vivo. The origins of pacemaker firing differ amongst various neuronal types. Thus, brainstem dopaminergic neurons may fire regularly without excitatory synaptic input [24, 25]. Mathematical modeling showed that the rhythmic activity is driven by subthreshold oscillations arising from an interplay between an L-type calcium current and a calcium-activated potassium current [26].

The mechanisms of pacemaker firing in LC neurons are not fully understood, although it can be sustained by a TTX-insensitive persistent sodium current [27, 28]. For serotonergic neurons of the DRN, there have been no reports of a persistent sodium current and L-type calcium currents are relatively small or absent [29], so the main candidate for depolarization underlying pacemaking is a combination of T-type calcium current and the classical fast TTX-sensitive sodium current which dominates the pre-spike interval [30]. In some cells, the hyperpolarization-activated cation current may also play a role.

In **Figure 1** are shown portions of spike trains in mouse and rat LC and rat DRN and CRN. Notably, the frequency of firing of LC and DRN principal neurons depends on the sleep stage. Thus, for example, in rats, waking, slow-wave sleep and REM sleep are accompanied by LC firing rates of about 2.2 Hz, 0.7 Hz and 0.02 Hz, respectively [31, 32, 33].

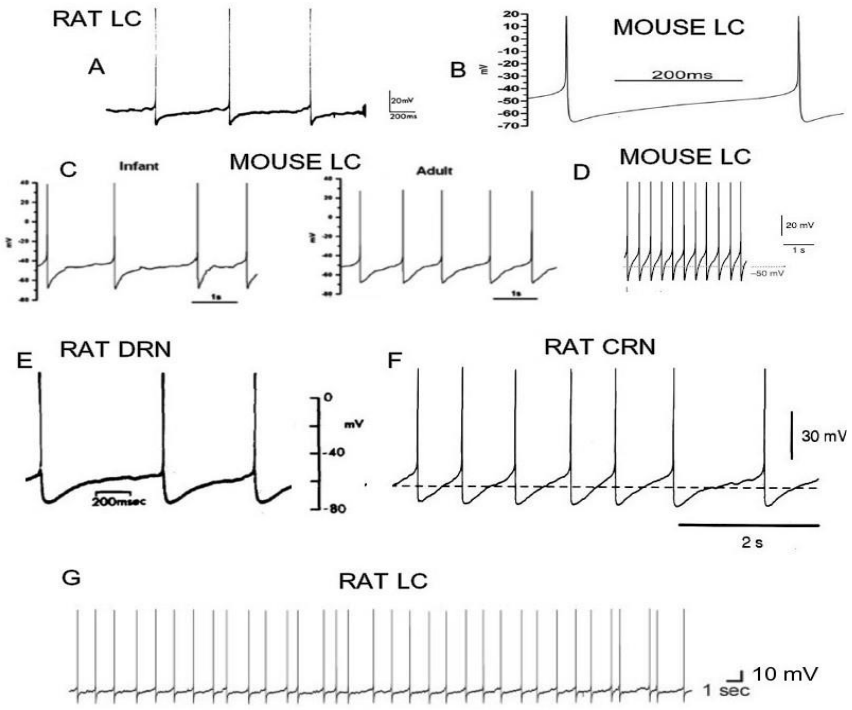

Figure 1*: Some representative spikes from rat and mouse raphe nuclei and LC neurons.* ***A****. Part of a train of spikes in a rat LC neuron in slice. Markers 20 mV and 200 ms [43].* ***B****. Detail of the course of the average membrane potential in a mouse LC neuron during an interspike interval [44].* ***C****. Action potentials in infant (7 to 12 days) and adult (8 to 12 weeks) mice [45].* ***D****. Whole-cell current-clamp recording of spikes in a mouse (21 to 32 days) LC neuron [5].* ***E****. A few spikes from rat dorsal raphe nucleus (slice) [46].* ***F****. Portion of a spike train from rat caudal raphe nucleus [47].* ***G****. Train of spontaneous spikes at a mean frequency of 0.85 Hz for a rat LC neuron in vitro [48].*

Figure 2 shows spikes computed with the detailed model of rat DRN SE neurons [30] for four different parameter sets. This model's key variables include membrane potential and intracellular calcium ion concentration, which satisfy ordinary differential equations. However, 11 distinct membrane currents drive the system, resulting in a dynamical system with 18 components and over 120 parameters.

To study network properties and quantities such as ISI distributions with various sources of random synaptic input, it is helpful to have a simpler system of differential equations that might yield insight into the properties of the detailed model whose execution with random inputs over hundreds of trials would be overly time-consuming. It is also pointed out that LC and DRN principal neurons are responsive to activation of about 20 different receptor types, as exemplified by those on DRN SE neurons - see Section 5.2. Including many such afferents makes computational tasks even more cumbersome with an 18-component neuron model [34, 35].

Simplified models of spike generation would also be useful in modeling the dynamics of serotonin release and uptake [36].

Approximating neuronal dynamics with such models, including the well-known leaky integrate and fire model and linear cable models, has been proven useful in other contexts by several authors, some of whom reduced the number of component currents (for example [37,38,39]) whereas others have simplified the geometry of the dendritic tree [40,41,42].

2. Description of a reduced two-component model

A first goal was to construct a two-component differential equation model whose solutions for the membrane potential broadly mimicked those for the multi-dimensional model developed in [30], which had given satisfactory agreement with experimental voltage trajectories (see references in [30]).

To this end, the following pair of equations with suitable choice of parameters had solutions with the desired properties. Here *V*, in m*V*, *V* is the depolarization of membrane potential from the resting value, and R is a recovery variable.

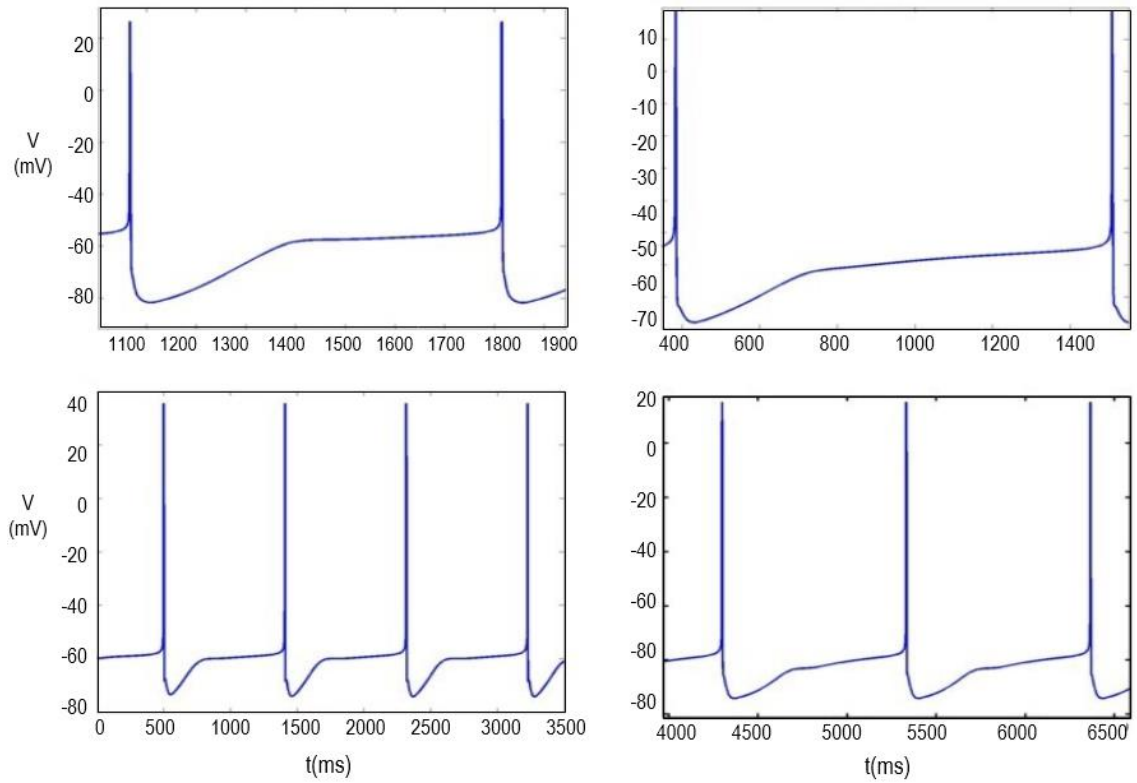

Figure 2*: Examples of computed spikes in a model for serotonergic neurons of the rat dorsal raphe nucleus from the model of Tuckwell and Penington [30]. Illustrated is the prolonged after hyperpolarization after a spike. The subsequent climb to the threshold is plateau-like, sometimes being almost horizontal. Membrane potentials in mV are plotted against time in ms.*

In keeping with the properties of the variables in the Fitzhugh-Nagumo equations (see [49] Section 8.8), R will be (arbitrarily) ascribed units of mV/ms. Then we have

$$\frac{dV}{dt} = \frac{1}{a}(V - V_1)(V - V_2)(V_3 - V) - \lambda R + I_{App} \quad (1)$$

$$\frac{dR}{dt} = \frac{\epsilon}{1+\exp\left[\frac{-(V-V_a)}{k_a}\right]} + kRV, \quad (2)$$

which system is usually to be solved with the initial conditions $V(0) = V_0$, $R(0) = R_0$. The initial value of V is usually set at the resting membrane potential so that $V_0 = V_R$, whose average value for DRN SE neurons is -64.4 mV [50].

To study spiking, it will be assumed that the parameters α, λ, ϵ, k and k_a are positive. The zeros of the cubic

$$f(V) = \frac{1}{a}(V - V_1)(V - V_2)(V_3 - V) \quad (3)$$

Are chosen such that $V_1 < V_2 < V_3$, with $V_1 < 0$ and $V_2 < 0$.

3. Examples of results for the two-component model

In this section, we give examples of computed solutions for the above two-component system and consider some of the properties of the solutions.

Examples with two sets of parameters

There are ten parameters for the system of equations (1) and (2). Here we describe solutions for two sets of parameters, whose values are listed in **Table 1**. The solutions for both sets consist of periodic solutions in V and R, where the first component mimics trains of action potentials.

For parameter set 1, the (numerical) solutions are shown in **Figure 3A,** and some of the details of the solutions, such as maximum and minimum values of V, mean ISI, and mean duration, are measured at $V = -40$ mV. The maximum value of R is given in the second column of **Table 2.** These results were obtained using an Euler scheme with $\Delta t = 0.02$ ms.

The voltage trajectories resemble some of the experimental ones in **Figure 1,** particularly for rat and mouse LC neurons (A and C) and, to a lesser extent, the rat DRN neurons (E). The duration of action potential (measured at -40 mV) is only 0.55 ms, which is too short for these brainstem neurons. Furthermore, the AHP declines to a very low value of about -109 mV, which is 49 mV below the assumed resting level. To make the minimum considerably higher in accordance with most experimental values, it is noted that the minimum of V occurs when $dV/dt = 0$ or when

$$f(V) = \lambda R^* - I_{App} \quad (4)$$

where R^* is the value of R when the minimum of V occurs. The graphical situation is shown in **Figure 4.** By judicious choice of values of the parameters, it was possible to obtain periodic solutions with minima of V at an appropriate value of about -83 mV. This resulted in the parameter set 2, whose solution properties are displayed in **Figure 3B** and column 3 of **Table 2.** These results were also obtained using an Euler scheme with step 0.02. The corresponding results with a smaller step of $\Delta t = 0.005$ ms are given in column 4. A much smaller value of Δt should lead to more accurate solutions. Still, considering that the computing time was about 30 times longer and the change in solution properties such as ISI and duration was less than 1%, it is satisfactory here to use the larger time step. A comparison was also made with results obtained using a 4th order Runge-Kutta scheme, which was an order of magnitude slower than the Euler method and gave an almost identical ISI of 869.04 ms.

Table 1: Two sets of parameters for the system (1), (2)

Parameter	Set 1	Set 2	Parameter	Set 1	Set 2
α	400	400	V_1	-77.4	-60
ϵ	30	5	V_2	-61	-50
k_a	2	2	V_3	20	20
V_a	-10	-10	I_{App}	15	15
λ	60	20	k	0.00042	0.0000525

Table 2: Some details for the spike trains for sets 1 and 2 parameters with $I_{App} = 15$.

Property	Set 1	Set 2	Set 2
Δt	0.002 ms	0.002 ms	0.005 ms
Mean ISI (ms)	501.1	870.8	869.5
Mean Duration (ms)	0.55	2.81	2.79
Max *(V) (mV)*	+8.9	+18.7	+18.5
Min*(V) (mV)*	-109.4 *mV*	-83.5	-83.4
Max*(R)*	8.7	10.96	10.90

3.1 Frequency versus current curves

The above results for sets 1 and 2 parameters were obtained with $I_{App} = 15$. It is interesting to compute the frequency of action potentials for various applied currents, as this corresponds to certain experimental data. The plot of output frequency versus applied current is called an *f/I* curve which differs in its characteristics from neuron to neuron. Often there is a threshold current for action potentials, which in the classical literature was called the rheobase current.

Hodgkin [51] found that there were two broad types of *f/I* curves for squid axon preparations. Type 1 consisted of an *f/I* curve that smoothly rose from zero at a particular input current value, whereas type 2 curves discontinuously rose at a certain threshold current. Tateno et al. [52] found that regular spiking and fast-spiking neurons in the rat somatosensory cortex exhibit Type 1 and Type 2 firing behaviors, respectively. Mathematical explanations for the two types of thresholds are found, like the bifurcation, which accompanies the transition from a rest state to a periodic firing mode, as discussed in Section 4.

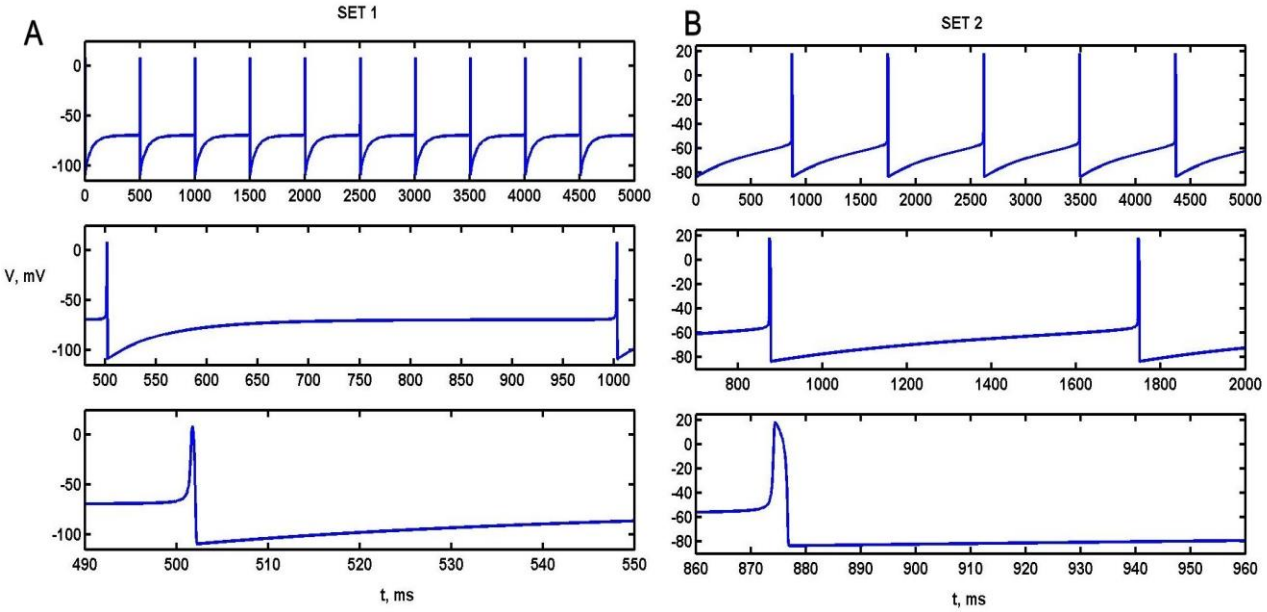

Figure 3*: A. Plots of numerical solutions for the two-component model with the first parameter set of Table 1. V (t) is plotted against t with three different timescales to show the spike train and spike details. B. Corresponding results for set 2 parameters.*

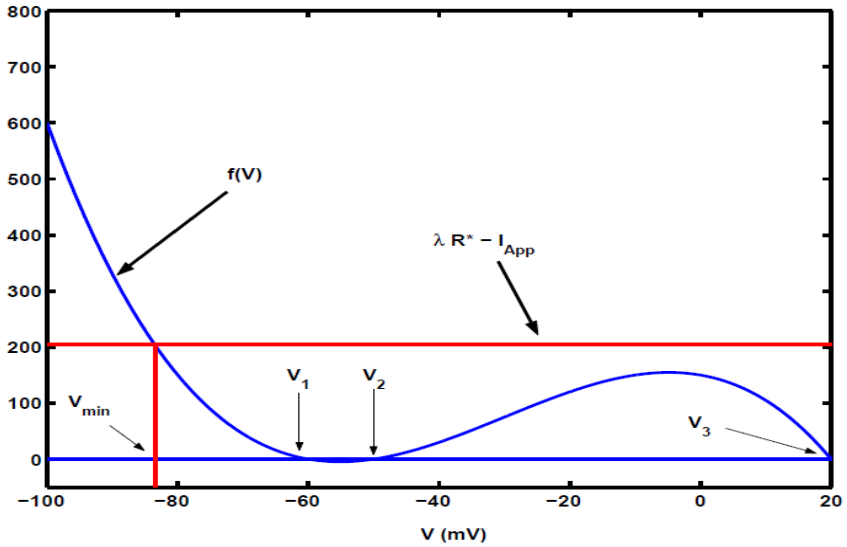

Figure 4*: Illustrating the graphical solution for the minimum of V.*

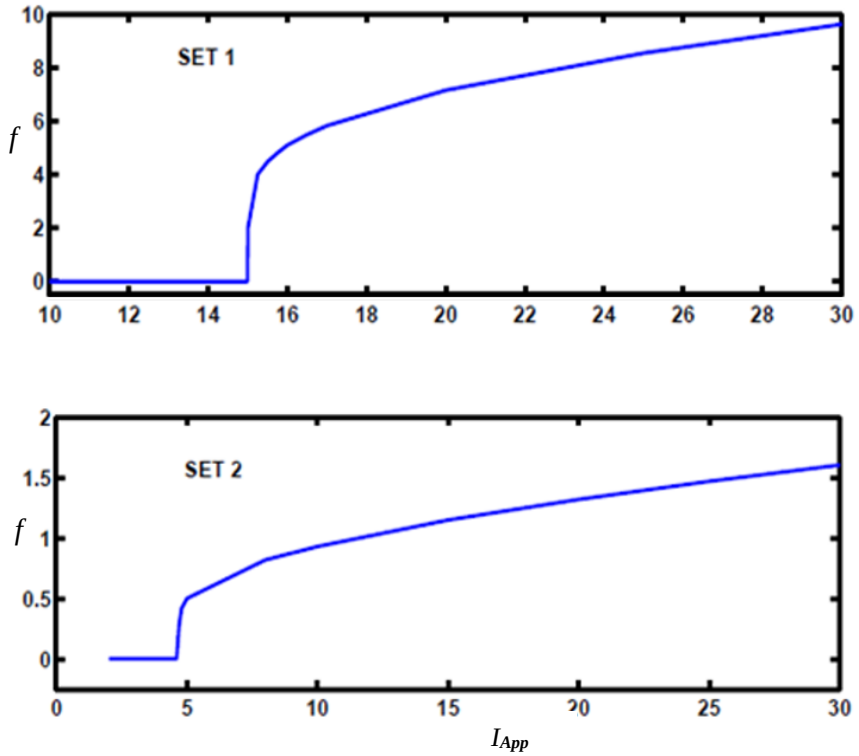

***Figure 5**: Frequency versus input depolarizing current for parameter sets 1 (above) and 2 (below).*

Graphs of the frequency of repetitive spiking versus depolarizing input current are shown in Figure 5 for parameter sets 1 and 2. In both cases, the frequency jumps from zero to a positive value at a particular value of the applied current I_{App}. For parameter set 1, the threshold current for firing is very close to 15, at which the firing frequency is about 2 Hz. For parameter set 2, the threshold current is about $I_{App} = 4.7$, where the firing frequency jumps from zero to about 0.29 Hz. Thus the responses of the model with either parameter set are those of type 2 neurons [51]. The nature of the *f/I* curves for the approximate model is thus similar to that for both the experimental results for DRN SE neurons and the multi-component model [30].

3.1.1 Autonomous pacemaker activity

The above results on frequency versus current indicate that to make the model neuron fire with parameter sets 1 and 2, current $I_{App} > 0$ must be applied. If $R(0) = 0$, this is necessary because the cubic f*(V)* defined in Eq. (3) is negative for a range of values of *V*, and in particular, the range containing *V(0)*. If $V_1 = V_2 = -60$, the cubic is tangential to the *V* -axis and *f(V)* is never negative.

Then firing, albeit very slow, was demonstrated to occur for values of I_{App} extremely close to zero, implying autonomous firing in the limit. It is possible by choosing a cubic *f(V)* with only one real root, for example, at $V_3 = 20$ (as in parameter sets 1 and 2), so that $f(V) > 0$ for all $V < V_3$, in which case autonomous firing could occur; that is with $I_{App} = 0$. The resulting source function would then be similar to the steady-state curve in Figure 18 of the multidimensional model [30], where in some cases, it was found that pacemaker firing occurred in some cases for $I_{App} = 0$ or even $I_{App} < 0$, whereas in others, a small depolarizing drive was necessary.

4. Effects of changing parameters and phase plane analysis

A detailed compilation of the effects on the spike train properties as each of the ten parameters is varied is not explored here. Instead, Table 3 lists the effects of increasing or decreasing each of the ten parameter values relative to their values in set 2 on the mean *ISI*, mean duration of spike, maximum and minimum of voltage during spike, and maximum value of the recovery variable during spiking.

We focus attention on the ISI and spike duration. For the ISI, significantly altering each of the parameters ϵ, λ, V_a and k_a had little or no effect. On the other hand, the ISI was increased by decreasing any of α, I_{App}, V_1 and k or by increasing either V_2 *or* V_3. The duration of spikes was little affected by significant changes in any of k, k_a, I_{app}, V_1, V_2 or by decreases in V_a. However, increases in V_a led to a substantial increase in duration. Significant increases in duration resulted from decreases in any of α, ϵ or λ, or increases in V_3.

To see the bifurcations involved when the injected current I_{App} is changed, we analyze the phase plane of the model. The two nullclines of the two-component model are

$$R = \frac{1}{\lambda a}(V - V_1)(V - V_2)(V_3 - V) + \frac{I_{App}}{\lambda} \tag{5}$$

for $dV/dt = 0$, and

$$R = -\frac{\epsilon}{1 + \exp\left[\frac{-(V - Va)}{k_a}\right]} \cdot \frac{1}{kV}, \tag{6}$$

for $dR/dt = 0$.

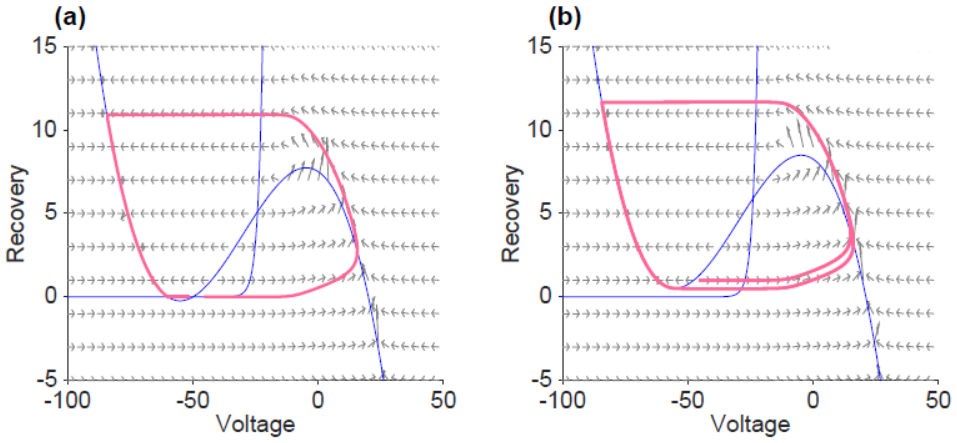

(c)

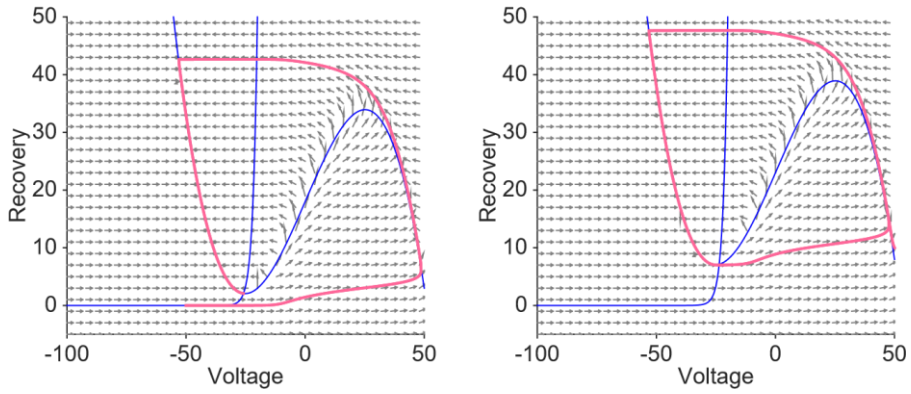

Figure 7: *Phase portraits of the two-component model for different parameters. In panel (a), $I_{App} = 0$, $\epsilon = 8$, while the other parameters are the same as set 2 in Table 1, and the resting state is a stable node. As I_{App} increases, the system goes through a saddle-node bifurcation. In panel (b), I_{App} is increased to 15, the system has only one equilibrium remaining, and there is a limit cycle. In panel (c), $V_1 = -30$, $V_2 = -20$, $V_3 = 50$, and other parameters coincide with those in panel (b). With this parameter set, the system has only one equilibrium, which is a stable node. As I_{App} is increased, the system goes through an Andronov-Hopf bifurcation, and the stable node loses stability to give birth to a limit cycle, such as the one in panel (d). In panel (d), $I_{App} = 40$, while the other parameters are the same as in panel (c).*

Table 3: Properties of the spike trains for different sets of parameters relative to set 2

Parameters	**Mean ISI**	**Mean Duration**	**Max(V)**	**Min(V)**	**Max(R)**
Set 2	869.04	2.74	18.37	-83.40	10.88
$\alpha = 2000$	462.4	3.0822	0.26	-91.92	4.53
$\alpha = 200$	1231.84	4.0267	19.69	-81.73	18.32
$\epsilon = 2$	849.32	5.47	19.84	-82.15	9.87
$\epsilon = 8$	884.04	2.005	17.01	-84.32	11.66
$\lambda = 10$	853.02	4.58	19.58	-82.40	20.14
$\lambda = 30$	881.76	2.085	17.23	-84.18	7.70
$I_{app} = 10$	1069	2.74	17.95	-83.40	10.63
$I_{app} = 20$	755.52	2.74	18.78	-83.40	11.13
$V_1 = -65$	1127.82	2.8667	18.59	-86.82	11.51
$V_1 = -55$	794.7	2.66	18.10	-80.15	10.27
$V_2 = -55$	771.76	2.812	18.62	-86.21	11.65
$V_2 = -45$	1128.26	2.7067	18.05	-80.78	10.14
$V_3 = -15$	815.24	2.52	13.10	-81.73	9.12
$V_3 = 25$	919.14	3.025	23.63	-84.99	12.80
$V_a = -20$	883.14	2.63	17.78	-84.23	11.59
$V_a = 0$	840.84	3.14	18.86	-81.82	9.62
$k_a = 1$	869.3	2.73	18.37	-83.42	10.90
$k_a = 3$	868.76	2.75	18.36	-83.38	10.87
$k = 0.0000325$	1396.54	2.74	18.37	-83.42	10.89
$k = 0.0000725$	632.26	2.74	18.37	-83.39	10.88

The system may have one equilibrium or three equilibria depending on the parameters. The voltage variable, V, for each equilibrium, satisfies the equation

$$\frac{1}{\lambda a}\ (V-V_1)(V-V_2)(V_3-V)+\frac{I_{App}}{\lambda}=-\frac{\epsilon}{1+\exp\left[\frac{-(V-V_a)}{k_a}\right]} \quad (7)$$

Solving equation (7) for the applied current I_{App}, we find that the system goes through a saddle-node bifurcation when I_{App} increases. In **Figure 6(a),** the voltage V in the equilibrium equation (7) is plotted with respect to the applied current I_{App}. As we can see from this figure, when $I_{App} = 0$, $\epsilon = 8$, and the other parameters are the same with parameter set 2, the system has three equilibria, visualized in **Figure 7(a)** by the intersection of the cubic V -nullcline and the R-nullcline. A nearby saddle accompanies a stable node in the lower voltage range. The stable node corresponds to the resting state, and the saddle sets a threshold for the initial voltage required for a (non-repetitive) spike. As the current I_{App} increases, the distance between the stable node and the saddle decreases. Eventually, the saddle and the node collide and annihilate each other through a saddle-node bifurcation, and the bifurcation diagram is as in **Figure 6(b)**. Once I_{App} is larger than the bifurcation value, there is only one equilibrium which is an unstable focus, and the system has a limit cycle (see **Figure 7(b)** where $I_{App} = 15$).

The system may also go through an Andronov-Hopf bifurcation when I_{App} increases. For example, when $I = 15$, $\epsilon = 8$, $V_1 = -30$, $V_2 = -20$, $V_3 = 50$, and all other parameters coincide with parameter set 2. The system has only one equilibrium: a stable focus corresponding to the resting state (see Figure 7(c)). When I_{App} is increased, the stable focus loses its stability, a limit cycle exists (see **Figure 7(d)**), and the model exhibits spiking behavior.

From the theory of dynamical systems [53], spiking is a sequitur to either a saddle-node bifurcation or an Andronov-Hopf bifurcation results in a neuron with Type 2 dynamics as was found in the numerically generated *f/I* curves of **Figure 5.**

5. Discussion

The realistic mathematical modeling of brainstem neurons, beyond that provided by extremely simplified models such as the leaky integrate and fire (or Lapicque) model [49], is useful for investigating the responses of these cells to their complex array of synaptic and other input and to construct and analyze complex networks involving these cells and those in other centers such as the hippocampus, frontal cortex and hypothalamus.

5.1LC NA neurons

These neurons innervate widespread targets throughout the central nervous system and play a fundamental role in response to threats and stressors. Persistent stress leads to an amplified response in LC neurons which may underlay the occurrence of pathological anxiety [54]. Interestingly the number of efferent signals from LC neurons exceeds the number of afferent inputs. In a study of rhesus macaques [55], LC neurons displayed a transient activation when initiating an action and when exerting force. These findings were relevant to the involvement of the noradrenergic system in pathologies such as Parkinson's disease and depression, where actions are impaired. In another recent study of the importance of LC neurons in models of prodromal Parkinson's disease [56], increases were found in the autonomous pacemaker frequency of LC neurons, accompanied by changes in the magnitude of the after hyperpolarization.

There have been several mathematical models of locus coeruleus neurons per se, which include a few ionic channels ([57], abstract only) or many ionic channels, including the usual sodium and potassium, high and low threshold calcium currents, transient potassium I_A, persistent sodium, leak and hyperpolarization-activated cation current I_h ([27,28, 58]. Noteworthy is the omission of I_A in the model of [28] and its inclusion in [27] and [58]. Also, a persistent sodium current is included in [27] and [28] but not in [58].

Despite such uncertainties in the mechanisms involved in pacemaker activity in LC neurons, some of these works have included synaptic input and gap-junction inputs from neighboring LC neurons. The pioneering article of De Carvalho et al. [27] addressed the mechanisms of morphine addiction. It included several biochemical reactions involving cAMP, μ-opioid receptors, morphine, G-protein, AC, CREB and Fos. Tuckwell [59] contains an

unpublished summary of previous LC modeling and a review of LC neuron anatomy and physiology. Brown et al. [60] employed Rose-Hindmarsh model neurons to study a network of LC neurons, but there have not appeared any plausible simplified models for these cells per se. Thus the two-component models considered in this article may provide a starting point for investigating, for example, the effects of synaptic inputs on LC firing.

5.2 DRN SE neurons

These neurons also innervate widespread targets in the brain, including the cerebral cortex, striatum, amygdala, hypothalamus, substantia nigra and ventral tegmental area. They also target a broad set of inputs from within and exterior to the DRN - see Table 4.

In [62], an extensive modeling and experimental study of DRN neurons and networks containing them were carried out. The DRN neurons were described by generalized integrate and fire models, which required only a few parameters that could be estimated accurately. Such model neurons, whose spike trains are temporally inhomogeneous Poisson processes, were used to study networks of DRN serotonergic neurons and GABAergic neurons. A key finding was that the serotonergic neurons encoded the derivatives of their inputs.

For serotonergic neurons of the dorsal raphe nucleus, there has been only one detailed model as described in the introduction [30]. Note that although there are no reports of persistent *NaV* 1.6 or 1.7 type currents, there is evidence of long-term inactivation of the classical *NaV* 1.1-1.3 type channel [63].

Table 4: Receptors on DRN SE neurons and adjacent presynaptic terminals

Symbol	Ligand	Symbol	Ligand
D2	Dopamine	GR	Cortisosterone
ACH-N (Nicotonic)	Acetylcholine	α_1	Noradrenaline
α_2	Noradrenaline	Glycine	Glycine
AMPA	Glutamate	NMDA	Glutamate
5-HT1A	Serotonin	OX-R1, OX-R2	Orexin
CRF-R1, CRF-R2	CRF	H-R1, H-R2	Histamine
K	opioids (morphine)	μ	opioids
CB1	Substance P	$GABA_A$	GABA
$GABA_B$	GABA	NPS	Neuropeptide S
MCH-1	Melanocortin	5-HT1B	Serotonin

In addition to their role in functions such as sleep-wake cycles, feeding behavior and mood, the serotonergic neurons of the DRN are involved in many cognitive functions. It is of great interest that the DRN serotonergic neurons and those of the dopamine reward system receive common inputs which point to a DRN role in reward processing - see [61] and references therein. Such involvement has been investigated in monkeys with single-unit recording [61], which indicated that DRN neurons responded to both the reward-predicting stimulus and the reward itself. In contrast, dopamine neurons predominantly responded only to the reward-predicting stimulus. Further, some DRN neurons respond to large and small rewards in distinction to dopamine neurons which tend to be excited only by large rewards.

Some authors have addressed serotonin release quantitatively and included the effects of antidepressants but without an explicit model for SE cell spiking [64]. Wong-Lin et al. [65] used a quadratic integrate and fire model for spiking DRN SE neurons in a network of such cells along with inhibitory neurons. The model is not vastly different from the model in this article, except that the reset mechanism after spikes is artificial. In related work, Cano-Colino et al. [66,67] have modeled the influence of serotonin on networks of excitatory and inhibitory cells in spatial working memory. More recently, in a similar vein, Maia and Cano-Colino [68] have made an interesting study of serotonergic modulation of the strength of attractors in the orbitofrontal cortex and related this to the occurrence of OCD.

6. Concluding remarks

Principal brainstem neurons, particularly serotonergic cells of the dorsal raphe nucleus and noradrenergic cells of the locus coeruleus, are of great importance in the functioning of many neuronal populations throughout cortical and subcortical structures. Of note is the modulatory role the firing of neurons in these brainstem nuclei have on neurons of the prefrontal cortex, including the orbitofrontal cortex and hippocampus. These latter structures have been strongly implicated in various pathologies, including depression and OCD. Lanfumey et al. [12] contain a comprehensive summary of many of the biological processes influenced by serotonin, including those originating from serotonergic neurons of the DRN. Modeling networks involving serotonergic and noradrenergic afferents requires plausible models for the spiking activity of the principal SE and NA cells. Whereas detailed models of such activity are now available, their application to many thousands of cells has the disadvantage of leading to very large computation time and large memory requirements, so the simplified models described in the present article may provide useful approximating components for such complex computing tasks.

Abbreviations

5-HT, 5-hydroxytryptamine (serotonin); AC, adenylate cyclase; AHP, afterhyperpolarization; cAMP, cyclic adenosine monophosphate; CREB, cAMP response element binding protein; CRH, corticotropin-releasing hormone; CRN, caudal raphe nucleus; DRN, dorsal raphe nucleus; EPSP, excitatory post-synaptic potential; GABA, gamma-aminobutyric acid; Hz, hertz; HPA, hypothalamus-pituitary-adrenal; ISI, interspike interval; LC, locus coeruleus; MDD, major depressive disorder; NA, noradrenaline or noradrenergic; OCD, obsessive-compulsive disorder; PTSD, post-traumatic stress disorder; PVN, paraventricular nucleus (of hypothalamus); REM, rapid eye movement; SE, serotonin or serotonergic.

Acknowledgements

This research was supported through an adjunct professorship to the University of Adelaide.

Conflict of Interest

The authors declare no conflict of interest

References

[1] Ramirez, J-M., Koch, H., Garcia, A.J. III, et al. (2011) The role of spiking and bursting pacemakers in the neuronal control of breathing. *Journal of Biological Physics* **37**, 241-261.

[2] Pan, W.J., Osmanovi´c, S.S., Shefner, S.A. (1994) Adenosine decreases action potential duration by modulation of A-current in rat locus coeruleus neurons. *Journal of Neuroscience* **14**, 1114-1122.

[3] Williams, J.T., Egan, T.M., North, R.A. (1982) Enkephalin opens potassium channels on mammalian central neurons. *Nature* **299**, 74-77.

[4] Ishimatsu, M., Williams, J.T. (1996) Synchronous activity in locus coeruleus results from dendritic interactions in pericoerulear regions. *Journal of Neuroscience* **16**, 5196-5204.

[5] Sanchez-Padilla, J., Guzman, J.N., Ilijic, E. et al. (2014) Mitochondrial oxidant stress in locus coeruleus is regulated by activity and nitric oxide synthase. *Nature Neuroscience* **17**, 832-842.

[6] Aghajanian, G.K., Vandermaelen, C.P. (1982) Intracellular recordings from serotonergic dorsal raphe neurons: pacemaker potentials and the effect of LSD. *Brain Research* **238**, 463-469.

[7] Aghajanian, G.K., Vandermaelen, C.P., Andrade, R. (1983) Intracellular studies on the role of calcium in regulating the activity and reactivity of locus coeruleus neurons in vivo. *Brain Research* **273**, 237-243.

[8] Alreja, M., Aghajanian, G.K. (1991) Pacemaker activity of locus coeruleus neurons: whole-cell recordings in brain slices show dependence on cAMP and protein kinase A. *Brain Research* **556**, 339-343.

[9] Williams, J.T., North, R.A., Shefner S.A. et al. (1984) Membrane properties of rat locus coeruleus neurones. Neuroscience **13**, 137-156.

[10] Lopez. J.F., Akil, H., Watson, S.J. (1999) Neural circuits mediating stress. *Biological Psychiatry* **46**, 1461-1471.

[11] Carrasco, G.A., Van de Kar, L.D. (2003) Neuroendocrine pharmacology of stress. *European Journal of Pharmacology* **463**, 235-272.

[12] Lanfumey, L., Mongeau, R., Cohen-Salmon, C., Hamon, M. (2008) Corticosteroid-serotonin interactions in the neurobiological mechanisms of stress-related disorders. *Neuroscience and Biobehavioral Reviews* **32**, 1174-1184.

[13] Mahar, I., Bambico, F.R., Mechawar, N., Nobrega J.N. (2014) Stress, serotonin, and hippocampal neurogenesis in relation to depression and antidepressant effects. *Neuroscience Biobehavioral Reviews* **38**, 173-192.

[14] Lowry, C.A., Rodda, J.E., Lightman, S.L., Ingram, C.D. (2000) Corticotropin- releasing factor increases in vitro firing rates of serotonergic neurons in the rat dorsal raphe nucleus: evidence for activation of a topographically organized mesolimbocortical serotonergic system. *Journal of Neuroscience* **20**, 7728-7736.

[15] Valentino, R.J., Foote, S.L., Page, M.E. (1993) The locus coeruleus as a site for integrating corticotropin-releasing factor and noradrenergic mediation of stress responses. *Annals New York Academy of Science* **697**, 173-188.

[16] Nestler, E. J., Alreja, M., Aghajanian, G.K. (1999) Molecular control of locus coeruleus neurotransmission. *Biological Psychiatry* **46**, 1131-1139.

[17] Jo¨els, M, Karst, H., Krugers, H.J., Lucassen, P.J. (2007) Chronic stress: Implications for neuronal morphology, function and neurogenesis. *Frontiers in Neuroendocrinology* **28**, 72-96.

[18] Swanson, L.W. (1976) The locus coeruleus: a cytoarchitectonic, Golgi and immunohistochemical study in the albino rat. *Brain Research* **110**, 39-56.

[19] Berridge, C.W., Waterhouse, B.D. (2003) The locus coeruleusnoradrenergic system: modulation of behavioral state and state-dependent cognitive processes. *Brain Research Reviews* **42**, 33-84.

[20] Jacobs, B.L., Azmitia, E.C. (1992) Structure and function of the brain serotonin system. *Physiological Reviews* **72**, 165-229.

[21] Vertes, R.P., Crane, A.M. (1997) Distribution, quantification, and morphological characteristics of serotonin-immunoreactive cells of the supralemniscal nucleus (B9) and pontomesencephalic reticular formation in the rat. *Journal of Comparative Neurology* **378**, 411-424.

[22] Vasudeva, R.K., Waterhouse, B.D. (2014) Cellular profile of the dorsal raphe lateral wing sub-region: relationship to the lateral dorsal tegmental nucleus. *Journal of Chemical Neuroanatomy* **57-58**, 15-23.

[23] Lowry, C.A., Evans, A.K., Gasser, P.J. et al. (2008) Topographic organization and chemoarchitecture of the dorsal raphe nucleus and the median raphe nucleus. In: *Serotonin and sleep: molecular, functional and clinical aspects*, p 25-68, Monti, J.M. et al., Eds. Basel: Birkhauser Verlag AG.

[24] Grace, A. A., Bunney, B.S. (1983) Intracellular and extracellular electrophysiology of nigral dopaminergic neurons. I. Identification and characterization. *Neuroscience* **10**, 301-315.

[25] Harris, N.C., Webb, C., Greenfield, S.A. (1989) A possible pacemaker mechanism in pars compacta neurons of the guinea-pig substantia nigra revealed by various ion channel blocking agents. *Neuroscience* **31**, 355362.

[26] Amini, B., Clark, J.W. Jr, Canavier, C.C. (1999) Calcium dynamics underlying pacemaker-like and burst firing oscillations in midbrain dopaminergic neurons: A computational study. *Journal of Neurophysiology* **82**, 2249-2261

[27] De Carvalho, L.A.V., De Azevedo, L.O. (2000) A model for the cellular mechanisms of morphine tolerance and dependence. *Mathematical and Computational Modelling* **32**, 933-953.

[28] Alvarez, V.A., Chow, C.C., Van Bockstaele, E.J., Williams, J.T. (2002) Frequency-dependent synchrony in locus ceruleus: role of electrotonic coupling. *Proceedings of the National Academy of Sciences (USA)* **99**, 4032-4036.

[29] Penington, N.J., Kelly, J.S., Fox, A.P. (1991) A study of the mechanism of Ca2+ current inhibition produced by serotonin in rat dorsal raphe neurons. *Journal of Neuroscience* **I7**, 3594-3609.

[30] Tuckwell, H.C., Penington, N.J. (2014) Computational modeling of spike generation in serotonergic neurons of the dorsal raphe nucleus. *Progress in Neurobiology* **118**, 59-101.

[31] Foote, S.L., Aston-Jones, G., Bloom, F.E. (1980) Impulse activity of locus coeruleus neurons in awake rats and monkeys is a function of sensory stimulation and arousal. *Proceedings of the National Academy of Sciences (USA)* **77**, 3033-3037.

[32] Aston-Jones, G., Bloom, F.E. (1981) Activity of norepinephrine containing locus coeruleus neurons in behaving rats anticipates fluctuations in the sleep-waking cycle. *Journal of Neuroscience* **1**, 876-886.

[33] Luppi. P-H., Clement, O., Sapin, E. et al. (2012) Brainstem mechanisms of paradoxical (REM) sleep generation. *European Journal of Physiology* **463**, 43-52.

[34] Kubista, H., Boehm, S. (2006) Molecular mechanisms underlying the modulation of exocytotic noradrenaline release via presynaptic receptors. *Pharmacology & Therapeutics* **112**, 213-242.

[35] Maejima, T., Masseck, O.A., Mark, M.D., Herlitze, S. (2013) Modulation of firing and synaptic transmission of serotonergic neurons by intrinsic G protein-coupled receptors and ion channels. *Frontiers in Integrative Neuroscience* **7**, 40.

[36] Flower, G., Wong-Lin, K. (2014) Reduced computational models of serotonin synthesis, release and reuptake. *IEEE Transactions on Biomedical Engineering* **61**, 1054-1061.

[37] Fitzhugh, R. (1961) Impulses and physiological states in theoretical models of nerve membrane. *Biophysical Journal* **1**, 445-466.

[38] Nagumo, J. S., Arimoto, S., Yoshizawa, S. (1962). An active pulse transmission line simulating nerve axon. *Proceedings of I.R.E.* **50**, 2061-2070.

[39] Destexhe, A., Rudolph, M., Fellous, J-M., Sejnowski, T.J. (2001) Fluctuating synaptic conductances recreate in vivo-like activity in neocortical neurons. *Neuroscience* **107**, 13-24.

[40] Rall, W. (1962) Theory of physiological properties of dendrites. *Annals New York Academy of Science* **96**, 1071-1092.

[41] Walsh, J.B., Tuckwell, H.C. (1985) Determination of the electrical potential over dendritic trees by mapping onto a nerve cylinder. *Journal of Theoretical Neurobiology* **4**, 27-46.

[42] Bush, P.C., Sejnowski, T.J. (1993) Reduced compartmental models of neocortical pyramidal cells. *Journal of Neuroscience Methods* **46**,159-166.

[43] Andrade. R., Aghajanian, G.K. (1984) Locus coeruleus activity in vitro: intrinsic regulation by a calcium-dependent potassium conductance but not α2-adrenoceptors. *Journal of Neuroscience* **4**, 161-170.

[44] De Oliveira, R.B., Howlett, M.C.H., Gravina, F.S. et al. (2010) Pacemaker currents in mouse locus coeruleus neurons. *Neuroscience* **170**, 166177.

[45] De Oliveira, R.B., Gravina, F.S., Lim, R. et al. (2011) Developmental changes in pacemaker currents in mouse locus coeruleus neurons. *Brain Research* **1425**, 27-36.

[46] Vandermaelen, C.P., Aghajanian, G.K. (1983) Electrophysiological and pharmacological characterization of serotonergic dorsal raphe neurons recorded extracellularly and intracellularly in rat brain slices. *Brain Research* **289**, 109-119.

[47] Bayliss, D.A., Li, Y.-W., Talley, E.M. (1997) Effects of serotonin on caudal raphe neurons: activation of an inwardly rectifying potassium conductance. *Journal of Neurophysiology* **77**, 1349-1361.

[48] Jedema, H.P., Grace, A.A. (2004) Corticotropin-releasing hormone directly activates noradrenergic neurons of the locus ceruleus recorded in vitro. *Journal of Neuroscience* **24**, 9703-9713.

[49] Tuckwell, H.C. (1988) Introduction to *Theoretical Neurobiology*. Cambridge University Press, Cambridge UK.

[50] Tuckwell, H.C. (2013) Biophysical properties and computational modeling of calcium spikes in serotonergic neurons of the dorsal raphe nucleus. *BioSystems* **112**, 204-213.

[51] Hodgkin, A.L. (1948) The local changes associated with repetitive action in a non-medullated axon. *Journal of Physiology (London)* **107**, 165-181.

[52] Tateno, T., Harsch, A., Robinson, H.P.C. (2004) Threshold firing frequency-current relationships of neurons in rat somatosensory cortex: Type 1 and Type 2 dynamics. *Journal of Neurophysiology* **92**, 2283-2294.

[53] Ishikevich, E. M. (2007) *Dynamical Systems in Neuroscience: The Geometry of Excitability and Bursting*. MIT Press, Cambridge, Mass.

[54] Morris, L.S., McCall, J.G., Charney, D.S. and Murrough, J.W. (2020) The role of the locus coeruleus in the generation of pathological anxiety. *Brain and Neuroscience Advances* **4**, 1-18.

[55] Bornert, P. and Bouret, S. (2021) Locus coeruleus neurons encode the subjective difficulty of triggering and executing actions. *PLoS Biology* **19**, p.e3001487.

[56] Matschke, L.A., Komadowski, M.A., Sthr, A., Lee, B., Henrich, M.T., Griesbach, M., Rinn, S., Geibl, F.F., Chiu, W.H., Koprich, J.B. and Brotchie, J.M. (2022) Enhanced firing of locus coeruleus neurons and SK channel dysfunction are conserved in distinct models of prodromal Parkinson's disease. *Scientific Reports* **12**, 1-14.

[57] Putnam, R., Quintero, M., Santin, J. et al. (2014) Computational modeling of the effects of temperature on chemosensitive locus coeruleus neurons from bullfrogs. *FASEB Journal* **28**, Supp. 1128.3. (Abstract only).

[58] Carter, M.E., Brill, J., Bonnavion, P. et al. (2012) Mechanism for hypocretin-mediated sleep-to-wake transitions. *Proceedings of the National Academy of Sciences (USA)* **109**, E2635E2644.

[59] Tuckwell, H.C. (2015) Computational modeling of spike generation in locus coeruleus noradrenergic neurons. Preprint.

[60] Brown, E., Moehlis, J., Holmes, P. et al. (2004) The influence of spike rate and stimulus duration on noradrenergic neurons. *Journal of Computational Neuroscience* **17**, 13-29.

[61] Nakamura, K. (2013) The role of the dorsal raphe nucleus in reward-seeking behavior. *Frontiers in Integrative Neuroscience* **7**, 60.

[62] Harkin, E.F., Payeur, A., Lynn, M.B., Boucher, J.F., Caya-Bissonnette, L., Cyr, D., Stewart, C., Longtin, A., Naud, R. and Bque, J.C. (2022) Temporal derivative computation in the dorsal raphe network revealed by an experimentally-driven augmented integrate-and-fire modeling framework. bioRxiv, doi.org/10.1101/2021.06.25.449907. (preprint).

[63] Navarro, M.A., Salari, A., Lin, J.L., Cowan, L.M., Penington, N.J., Milescu, M. and Milescu, L.S. (2020) Sodium channels implement a molecular leaky integrator that detects action potentials and regulates neuronal firing. *Elife* **9**, p.e54940.

[64] Geldof, M., Freijer, J.I., Peletier, L.A. et al. (2008) Mechanistic model for the acute effect of fluvoxamine on 5-HT and 5-HIAA concentrations in rat frontal cortex. *European Journal of Pharmaceutical Sciences* **33**, 217-219.

[65] Wong-Lin, K-F., Joshi, A., Prasad, G., McGinnity, T.M. (2012) Network properties of a computational model of the dorsal raphe nucleus. *Neural Networks* **32**, 15-25.

[66] Cano-Colino, M., Almeida, R., Compte, A. (2013) Serotonergic modulation of spatial working memory: predictions from a computational network model. *Frontiers in Integrative Neuroscience* **7**, 71.

[67] Cano-Colino, M., Almeida, R., Gomez-Cabrero, D. et al. (2014) Serotonin regulates performance nonmonotonically in a spatial working memory network. *Cerebral Cortex* **24**, 2449-2463.

[68] Maia, T.V., Cano-Colino, M. (2015) The role of serotonin in orbitofrontal function and obsessive-compulsive disorder. *Clinical Psychological Science* **3**, 460-482, and Supplemental-data.